Article

Spatiotemporal Study of Iron Oxide Nanoparticle Monolayer Formation at Liquid/Liquid Interfaces by Using In Situ Small-Angle X-ray Scattering

Jiayang Hu, Evan W. C. Spotte-Smith, Brady Pan, Roy J. Garcia, Carlos Colosqui, and Irving P. Herman*

Read Online

ACCESS | Metrics & More | Article Recommendations | SI Supporting Information

ABSTRACT: Spatial and temporal small-angle X-ray scattering (SAXS) scans show that 8.6 and 11.8 nm iron oxide nanoparticles (NPs) in heptane drop-cast on top of a heptane layer atop a diethylene glycol (DEG) layer are trapped at the DEG/heptane interface to generally form a single ordered, hexagonal-close packed monolayer (ML), and this occurs long before the heptane evaporates. Many NPs remain dispersed in the heptane after this NP assembly. Assembly occurs faster than expected from considering only the diffusion of NPs from the drop-cast site to this liquid/liquid interface. The formation of the ordered NP ML occurs within 100 s of drop-casting, as followed by using the (10) ordered NP SAXS peak, and on the same time scale there is a concomitant decrease in the SAXS form factor from disordered NPs that is apparently from disordered NPs at the meniscus. Usually, most of the ordered NPs are close packed, but there is evidence that some are ordered although not close packed. After the heptane evaporates, a close-packed ordered NP ML remains at the DEG/vapor interface, though with smaller NP–NP separation, as expected due to less van der Waals shielding caused by the upper medium in the interface. X-ray beam transmission at different vertical heights characterizes the heptane and DEG bulk and interfacial regions, while monitoring the time dependence of SAXS at and near the DEG/heptane interface gives a clear picture of the evolution of NP assembly at this liquid/liquid interface. These SAXS observations of self-limited NP ML formation at the DEG/heptane interface are consistent with those using the less direct method of real-time optical reflection monitoring of that interface.
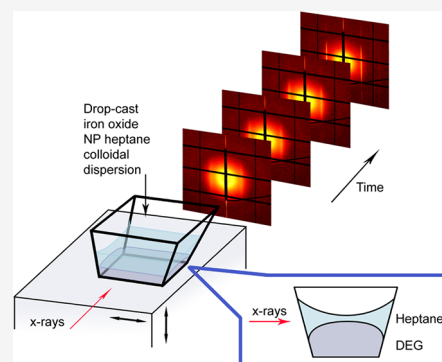
1. INTRODUCTION

Nanostructures can be fabricated by the self-assembly of nanoparticles (NPs) at a liquid surface, followed by transfer of the NP layer to another surface.[1−5] In a commonly used method, NPs dispersed in a solvent are drop-cast on a denser, less volatile, and immiscible lower solvent, and the number of NP layers remaining on the lower solvent after the upper one has evaporated depends on the number of NPs deposited during drop-casting.[4,5] A NP monolayer (ML) will remain, as is often desired,[5] only when the number of NPs in the drop-cast sample is carefully calibrated; this can also occur when conditions enable the use of miscible solvents, which is not always possible or desirable.[3] However, using the standard procedure with immiscible solvents, if after drop-casting some NPs assemble at the liquid/liquid interface before the upper liquid evaporates and if this assembly were limited to 1 ML, then this NP ML could be transferred and used, and there would be no need for careful NP drop-casting calibration.

The Pieranski model[6] has been widely used to estimate the binding energy of particles to fluid interfaces and has been used to account for the Pickering effect, the sometimes unexpected stability of bubbles and emulsions.[7] However, the ratio of this binding energy to the thermal energy decreases rapidly with particle size, and it is also sensitive to model parameters, details of the interface, and possibly important higher order binding effects, so it is not certain whether or not NPs will bind stably to particular liquid/liquid interfaces and that it will form only a single ML.[8] For example, this model predicts it is energetically favorable for oleate-capped iron oxide NPs to remain in the heptane solvent over binding to the diethylene glycol (DEG)/heptane interface.[5]

In earlier small-angle X-ray scattering (SAXS) measurements, we followed the NPs at the liquid/liquid interface, after 8.6−15.0 nm diameter iron oxide NP hexane or heptane colloidal dispersions were drop-cast on DEG liquid substrates, and concluded that the NPs remained in the upper solvent until it evaporated, and only then would a NP layer form on the DEG.[5] This was concluded because of the long time it took to see sharp SAXS peaks from ordered NP MLs at the DEG interface with the volatile hexane or heptane upper solvent, because such peaks were never observed with less volatile
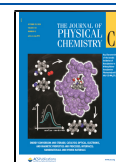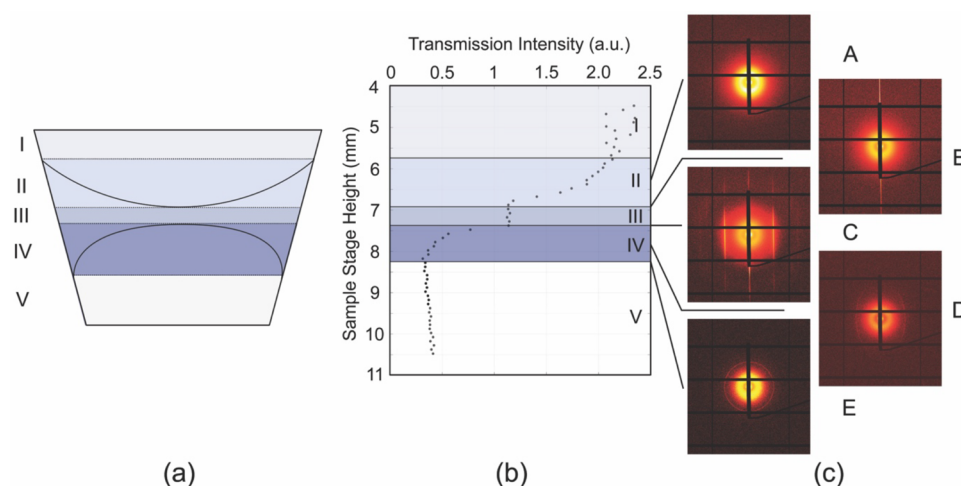
Figure 1. Geometry of the SAXS sample cell and measurements after 60 μL of 1 ML-equivalent 8.6 nm iron oxide NP heptane dispersion was autodropped on a heptane reservoir atop a DEG layer. The upper, heptane/vapor interface is concave up, and the lower, DEG/heptane interface is concave down, as shown in the cell schematic in (a). X-ray transmission was collected when the horizontal beam passed through the sample cell which was set on a vertically moving stage. The liquid in the cell is classified into five sections according to the different transmission intensity vs stage height curvature, as marked as I−V in both (a) and (b). Approximately 20 min after drop-casting, SAXS images were taken at different heights and are shown in (c).

upper solvents, such as decane, and because of the apparent observation of hexane or heptane evaporation occurring in similar times in analogous experiments in Petri dishes by using optical microscopy. Given this, the potential sensitivity to experimental conditions, and the uncertainties in the model parameters,[5] the direct examination of the NPs with SAXS within each phase and interface as a function of time is warranted.

Such an investigation is also motivated by a recent study[9] in which we used real-time optical reflection monitoring near Brewster's angle after NP drop-casting, which suggested that a ML of 11.8 nm diameter iron oxide NPs indeed forms at the interface before the upper solvent evaporates. Moreover, this layer seemed to be limited to a ML of NPs even when many more than this number of NPs were drop-cast.

To understand the transport and kinetics of assembly issues more fully, as could be important in applications,[10−13] we investigated this process directly by using SAXS to probe the DEG/heptane interface and the heptane dispersion atop it after drop-casting the NP iron oxide dispersion, as a function of both position and time. This was one key new feature in this study. Another was to maintain good alignment of the SAXS X-ray beam with the DEG/heptane interface and to try to control the timing of the transport of NPs to this interface by remotely drop-casting the heptane NP dispersion on top of an existing heptane layer, the reservoir, which was atop a DEG layer. Being spatially integrated over the X-ray paths in the heptane dispersion and the DEG, including at the DEG/heptane interface, the SAXS scans could provide the following: (1) the relative number of disordered NPs in the dispersion and at the interface, by integrating over the form factor in wavevector q space, (2) the number of ordered NP MLs at the interface, by integrating over the sharp peaks arising from the order, and the degree of order, from the peak widths, (3) the interparticle distances in the ordered ML, and (4) the time dependence SAXS features, such as when ordered peaks first appear, their areas and widths vs time, ...

2. EXPERIMENTAL METHODS

Iron oxide NPs encapsulated by oleate ligands were synthesized using a previous method.[14] NPs with core diameters of 8.6 and 11.8 nm sizes were used, with their sizes determined by fitting their form factors obtained by the SAXS of free dispersed NPs (see Supporting Information Section S7). The sample cell used to assemble NP MLs on top of a DEG layer and perform in situ SAXS was designed with a wall angle of 75° to suppress the meniscus of the DEG/vapor interface on the window material of fluorinated ethylene propylene (FEP); this results in a nearly flat interface forming a 90° contact angle relative to the vertical axis of the sample cell of DEG on FEP.[15] Sample cells using this design have previously been shown to collect much larger signals and improve the degree of order visible in SAXS images of ordered iron oxide NP self-assembly on liquid/vapor interfaces.[15] This geometry enables limited X-ray exposure and so better time resolution and yields superior SAXS images of the final structure after the volatile solvents atop the DEG evaporated. A detailed schematic of the sample cell is shown in the Supporting Information Figure S1. The cell was set on a stage that could move horizontally and vertically relative to the X-ray beam direction at the National Synchrotron Light Source II 11-BM Complex Materials Scattering (CMS) Beamline (Supporting Information Figure S2).

When studying the time dependence of assembly, 2 mL of DEG was added into the sample cell to form the lower liquid substrate, a ~3.85 mm thick DEG layer, with the top surface of 54.33 mm × 11.33 mm. This was followed by adding 1 mL of pure heptane in the main runs to form an upper liquid substrate that is called the heptane reservoir. The reservoir would be an ~1.64 mm thick layer, with top surface of 54.72 mm × 11.73 mm, if the menisci were flat, but here corresponds to a ~0.50 mm separation of the top of the DEG/heptane and bottom of the heptane/vapor menisci, as measured by X-ray transmission. Then this was followed by drop-casting a much smaller volume, 60 μL, of the 8.6 or 11.8 nm core diameter iron oxide NP dispersion in heptane of selected concentration; this would be equivalent to a layer that is ~0.1 mm thick if flat,

and so to a meniscus separation of ∼0.6 mm. Then these two layers above the DEG mixed. A cap was placed atop the sample cell after dropping the pure heptane reservoir to minimize evaporation in the relevant time frames. This cell is better sealed than that used in Zhang et al.,[5] so upper solvent evaporation is slowed to better distinguish it from other time scales in assembly events and is also slowed due to using heptane here rather than hexane. Several comparison experiments were also conducted by drop-casting the NP dispersion directly on the DEG layer, which was the procedure used in ref 5.

One advantage of this two-step procedure in NP injection on an existing heptane reservoir atop the DEG is the spatial stability of the DEG/heptane interface after aligning the X-ray beam. After the DEG is first added to the cell, a flat DEG/vapor interface forms due to the design of the cell. (If the cell had vertical walls, this interface would have been concave up.) After heptane is added and before it evaporates, the DEG interface moves, and the lower, DEG/heptane interface becomes concave down and the upper, heptane/vapor interface becomes concave up, as portrayed in Figure 1a. The X-ray beam was then aligned relative to the DEG/heptane interface before the NPs were drop-cast. In Zhang et al.,[5] the heptane dispersion was directly drop-cast on the DEG/vapor interface, so the X-rays needed to be realigned very quickly to the DEG/heptane interface; it is possible that the beginning of ML formation at the interface was missed due to this. In the current study, the speed of the X-ray beam alignment to the DEG/heptane after adding pure heptane, as described below, was not critical, and the shape and position of this interface, and so that of X-ray alignment, did not change, and assembly at the DEG/heptane interface could be followed immediately. Furthermore, the second step in this two-step injection of heptane provided a "delta function" NP concentration at $t = 0$ at the heptane/vapor interface, ∼2 mm away above the center of the heptane surface, and so transport to the DEG/heptane interface and NP layer formation at this interface could in principle be resolved more cleanly. Turbulence near the DEG interface was probably lessened by using this smaller volume and vertically displaced heptane dispersion.

The NPs were drop-cast after the heptane dispersion was loaded into PTFE tubing with inner diameter 0.79 mm by remote injection via an autoinjector (Digital Controlled Infusion Syringe Pump EQ-300SP-H-LD). The end of this tubing was set very near, $h \sim 2$ mm above the heptane/vapor interface to lessen the impact of the falling drop on NP transport in the heptane, an attempt at "gentle" drop-casting. The tubing went through the small hole on the cap and so was set near the center of the cell horizontally. Drop-cast NP concentrations are presented in terms of "ML-equivalents," defined as the number of MLs that would be expected to form on the DEG layer, after drop-casting and subsequent evaporation of heptane to form a flat DEG/vapor interface, in the Petri dish measurement vessel with dimensions similar to the SAXS sample cell; these are approximately, but not exactly, the number of MLs that could form for each experimental condition. For 8.6 nm NPs, this measured, calibration 1.0 ML-equivalent corresponded to ∼1.45 MLs of close-packed ordered NPs on the curved, concave down DEG/heptane interface and ∼1.09 MLs on the flat DEG/vapor interface in the SAXS sample cell, and for 11.8 nm it corresponded to ∼1.25 MLs and ∼1.09 MLs respectively, as shown in the Supporting Information Section S3. This means

that drop-casting 0.69 (= 1.0/1.45) ML-equivalents of 8.6 nm NPs and 0.80 (= 1.0/1.25) ML-equivalents of 11.8 nm NPs would be expected to produce 1.0 ML of hexagonal close-packed NPs at the DEG/heptane meniscus in the SAXS sample cell. For the 8.6 nm iron oxide NP studies, 0.2−12 ML-equivalents were drop-cast, and for 11.8 nm NPs, 0.2−18 ML-equivalents were drop-cast. Even during injection, the sample cell was sealed off from the environment to slow down heptane evaporation.

The X-ray wavelength was 0.9184 Å (13.5 keV), unless otherwise stated, and the cross section was 50 μm (vertical, x axis) × 200 μm (horizontal, y axis), with the sample being in the y−z plane (Supporting Information Figure S2). SAXS measurements used an X-ray detector array (DECTRIS Pilatus 2M) placed 3 m away, with 1475 × 1679 pixels, each with 3.90 × 10^{-3} nm^{-1} width. The lateral dimensions and curvatures of the DEG/heptane interface shift and broaden the SAXS signals by less than a pixel in the x and y directions. The finite length of the scattering region along the flat DEG/vapor interface also affects the signals by less than a pixel.

Before NP injection, X-ray beam transmission through the sample was measured as a function of sample cell height, as shown in Figure 1b. This enabled precise determination of the position of the DEG/heptane interface, so that time-resolved measurements could later be made at that interface nearly immediately after NP dispersion injection. This included X-ray transmission over a range of heights at and near each interface. Such a series of sequences of X-ray transmission scans took between 2 and 5 min, depending on the number of data points taken.

Runs with 8.6 nm iron oxide NPs with 0.5, 1, 3, 6, 9, and 12 ML-equivalents drop-cast and with 11.8 nm NPs with 6 ML-equivalents drop-cast were conducted with a strip beam stop for blocking (Supporting Information Figure S3a) to minimize noise and a 5 s exposure time for each beam position. In addition, survey runs during a previous visit to NSLS-II were conducted with 11.8 nm NPs and 1, 9, and 18 ML-equivalents drop-cast with 1 s exposure time and a very small circular beam stop (Figure S3b), both which led to results with increased noise.

For each run, after initial beam alignment, a series of SAXS measurements were conducted with the cell cyclically repositioned near the top of the DEG/heptane interface, which is the boundary of sections III and IV in Figure 1a, to ensure that the top of the DEG/heptane meniscus was being probed each time in this series, usually along with regions immediately above and below it. Each run consisted of repeated cycles, each with measurements at three heights separated by 50 μm, so if the alignment happened to be a bit off after the DEG/heptane interface was determined, the top of the meniscus was at least being probed in one of these three positions. In the runs during which 0.5, 1, 3, 9, and 12 ML-equivalents of 8.6 nm NPs and 6 ML-equivalents of 11.8 NPs were drop-cast, the position right above the top of the DEG/heptane meniscus was probed; in the runs in which 6 ML-equivalents of 8.6 nm NPs and 1, 9, and 18 ML-equivalents of 11.8 nm NPs were drop-cast, it was not probed, and so these runs are not shown below in Figure 5. The three targeted positions in a cycle were at the top of the meniscus and either (a) 50 μm above and 50 μm below it, (b) 100 and 50 μm above it, or (c) 100 and 50 μm below it. For example, in the 8.6 nm NPs runs with 1, 3, and 12 ML-equivalents drop-cast, the first SAXS measurement was with the center of the beam

50 μm above the meniscus, and so the beam did not probe the interface at all and showed no sharp SAXS peaks due to ordering. The cell then was raised by 50 μm, so the 50-μm tall beam was relatively lowered by this amount and was then "at" the top of the DEG/heptane meniscus. Thus, approximately half of the beam was in the heptane and half in the DEG (Supporting Information Figure S6), and after NP ordering there were sharp SAXS peaks. Then the cell was raised by 50 μm so the center of the beam was 50 μm below the interface, and so the beam did not probe the top of the meniscus at all but still showed sharp SAXS peaks from regions probed away from the center because the hexagonally close-packed NP ML formed over the entire DEG/heptane interface (see Section 3.2 and Supporting Information Section S8). Then the cell was lowered by 100 μm, and the above/at/below the meniscus sequence was repeated again and again. The sequences in all of the cycles are detailed in Supporting Information Section S6.

Each SAXS measurement took 8 s for the 8.6 nm NP runs and 6 ML-equivalents run for 11.8 nm NPs (5 s exposure time and 3 s processing time at each position), and so the measurements at the top of the DEG/heptane meniscus in each cycle were separated by 24 s. Similarly, SAXS measurements took 4 s for the preliminary runs with 1, 9, and 18 ML-equivalents of 11.8 nm NPs (1 s exposure time and 3 s processing time at each position), and the measurements at the top of the DEG/heptane meniscus in each cycle were separated by 12 s. The series of cycles for each condition lasted for several hundred seconds. Monitoring the sharp SAXS peaks in these cyclic measurements helped keep the beam aligned at the meniscus and minimize variations in intensity of the ordered SAXS peak due to changes in the numbers of NPs probed and changes due to varying path lengths in heptane and DEG with differing X-ray absorption in the liquids. The SAXS collections at three positions in each cycle ensured that the time-resolved changes of how NPs self-assembled at the DEG/heptane interface were seen and offered space-resolved pictures for comparing SAXS signals at and above the top of the DEG/heptane meniscus. This X-ray position cycling and data collection began before NP dispersion autoinjection, which is at $t = 0$ below in Figures 2−4, so data collection began "immediately." Detailed data sets are presented with the beam aligned above and at the top of the DEG/heptane meniscus (see the analyses in Section 3.4).

SAXS NP form factor signals with the beam aligned above and at the top of the DEG/heptane meniscus were integrated along q_x from −0.0780 nm^{-1} (−20 pixel) to +0.0780 nm^{-1} (+20 pixel) and then fit from $q_y = 1.057$ to 1.598 nm^{-1} for the 8.6 nm NPs and $q_y = 0.745$ to 1.150 nm^{-1} for the 11.8 nm NPs. (Though the Porod invariant accessible via integrating over dq_xdq_ydq_z entails integrating in the third dimension, the q_z wave vector was almost the same throughout the q_x, q_y range analyzed in this small-angle measurement. Thus, it is reasonable to analyze SAXS intensities as a function of q_y after integration over a range of q_x.) Gaussian functions were used to fit the sharp (10) peaks after the background was removed; first a single Gaussian function was used, and then the sum of two Gaussian lineshapes was used for this fit. To account for the longer integration times for the 6 ML-equivalents of 11.8 nm NPs, SAXS intensities were divided by 5 when analyzed. The generally shorter integration times (and larger X-ray backgrounds) in the preliminary runs for the larger NPs led to smaller signal/noise ratios. In most cases, background SAXS images were taken near the top of the

DEG/heptane meniscus before the NPs were drop-cast, and then this background was removed during peak fitting after normalization. In other cases, SAXS collection immediately before the NPs were drop-cast was used as the background that was subtracted. (See Supporting Information Sections S9 and S10 for more information about background subtraction and timing, respectively.)

After a given series of measurements and when no more significant changes in the SAXS pattern were seen (~12 min), another vertical scan of lateral X-ray transmission traces was conducted at the center of the sample cell from section II until the beam hit section V, as in Figure 1a, to determine if and by how much the meniscus at the DEG/heptane interface had changed during the course of the experiment and to what degree the heptane layer had already evaporated. In most experiments the cell components and windows were sealed well, and the heptane evaporated very little. An experiment was repeated when this was not so. Approximately 20 min after NP autoinjection and hours before the heptane evaporated when the images, and so the NP structure at the DEG/heptane interface, had reached steady state, a series of SAXS measurements at different heights were taken for additional space-resolved information and to examine NP assemblies away from the top of the DEG/heptane meniscus at lower heights on the interface.

The NPs at the DEG surface were also examined later after the purposeful loss of heptane. This was accelerated by removing the sample SAXS cell from the beamline and then flowing nitrogen laterally over the uncovered top of the sample cell until no heptane was visible. This typically took ~1−2 h. Then, before any significant amount of the much-less volatile DEG had evaporated, the sample cell was reintroduced to the beamline stage, and X-ray transmission was measured in a vertical scan to determine the shape of the meniscus for the 1, 6, 9, and 12 ML-equivalent runs with the 8.6 nm NPs and the 1 and 9 ML-equivalent runs for the 11.8 nm NPs. The sample was then probed at the DEG/vapor interface using SAXS to identify regions with NPs present and the degree of order present in those regions. All was cleaned before the next series of runs were started.

3. RESULTS AND DISCUSSION

Results are presented for the comprehensive runs with 8.6 nm diameter iron oxide NPs and the one such run with 6 ML-equivalents of 11.8 nm NPs drop-cast, along with those of the less extensive, preliminary runs with these larger NPs.

3.1. Observations before NP Dispersion Injection on the Heptane Layer. Figure 1b shows a typical scan of X-ray transmission vs height for 1 mL of the pure heptane reservoir on top of 2 mL of DEG before the injection of the NP dispersion. Section I is the vapor region above the heptane layer. This transmitted intensity is the largest there and does not change with height. The transmission intensity in section II, which represents the heptane/vapor interface, decreases with lower height as the beam is sent through thicker regions of the heptane/vapor interface due to increased absorption by heptane. Section III is bulk heptane, so the intensity does not change with height, aside from slight changes due to the tapered wall, path length, and X-ray absorption. Section IV is the region of the DEG/heptane interface. Transmission decreases with lower height in this region because DEG absorbs the X-rays more strongly than does the heptane (given the DEG absorption coefficient at 13.5 keV is 164.3/m and
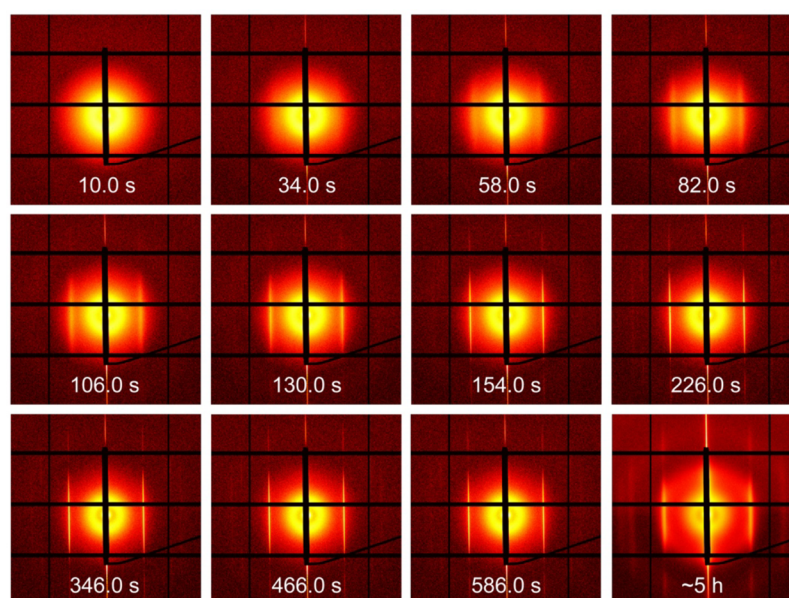
Figure 2. Evolution of time-resolved SAXS images at the top of DEG/heptane interface after 60 μL of 1 ML-equivalent 8.6 nm NP was autodropped onto the heptane reservoir. After more than 5 h—when the heptane reservoir was dry—SAXS was taken on the DEG/vapor interface, as shown in the last panel.

that of heptane is 55.94/m).[16] In section II in Figure 1b, the transmission intensity scan from a less absorptive phase (air) to a more absorptive phase (heptane) is concave up as plotted, and so the interface is concave up. In section IV, the transmission intensity scan from a less absorptive phase (heptane) to a more absorptive phase (DEG) is concave down as plotted, and so the interface is concave down. The DEG/heptane meniscus shape calculated in the Supporting Information Section S5 supports this conclusion. Section V is bulk DEG, with smaller X-ray transmission because DEG transmits X-rays less than does heptane. Transmission decreases slightly with increased height because the windows are at an angle, so the DEG layer is thicker along the beam direction with increased height for this cell.

The transmission data of Figure 1b were used to determine the shape of the DEG/heptane meniscus in Supporting Information Section S5, as seen in Figure S4; also see Section S6.

3.2. Formation of One Monolayer of Close-Packed NPs at the DEG/Heptane Interface: General SAXS Features. Figure 1c shows space-resolved SAXS images taken after the NP dispersion injection in a typical run (8.6 nm NPs, 1 ML-equivalent drop-cast). In section II, the SAXS image shows the NP form factor. This means that there are NPs in the heptane dispersion even when an ordered structure is formed below it at the DEG/heptane interface, as is seen below. At the bottom of the heptane/vapor interface (the section II/III boundary), the SAXS image indicates a reflection pattern at $q_y = 0$ from this liquid/vapor interface, as well as a form factor from the disordered dispersion of NPs. It is apparent that there are no ordered NPs at the heptane/vapor interface. At the top of the DEG/heptane interface (the section III/IV boundary), the SAXS image indicates a reflection pattern from this liquid/liquid interface, the form factor from NPs in the heptane region, and sharp peaks that indicate a well-ordered NP ML at this interface. Below this, in section IV, there are the form factor and curved sharp peaks that indicate an ordered 1 NP ML on a tilted interface (Figure 1c, part D;

Supporting Information Figure S10, top).[17] At the bottom of the DEG/heptane interface (the section IV/V boundary), the sharp peaks are nearly circular because the interface angle is steep (Figure 1c, part E; Supporting Information Figure S10, bottom).

The model by Smilgies et al.[18] is used to interpret the streak patterns. It combines the quasi-kinematic approximation with Vinyard theory to predict SAXS patterns for ordered MLs and 2−9 ML multilayers of NPs in close-packed arrangements. This model predicts a 1-ML SAXS pattern for a close-packed hexagonal arrangement that agrees with the sharp peak pattern seen in Figure 1. So, not only is the NP assembly at the DEG/heptane interface well-ordered, in contrast to the disordered NPs in the heptane bulk and the lack of NPs at the heptane/vapor interface, but it is also specifically 1 ML and close-packed, and not a multilayer.

3.3. The General Evolution of the Ordered NP Monolayer. Figure 2 shows the evolution of the SAXS images at the top of the DEG/heptane interface after NP injection for the run with core size 8.6 nm and 1 ML-equivalent drop-cast. Initially only the form factor is seen, and no ordering is visible. Then vertical streaks begin to appear, indicating two-dimensional order. The narrowing of these streaks indicates improved order, and the lattice spacing of the NP ML becomes well-defined and consistent. The relative positions of these continuous streaks are $1:\sqrt{3}:2:...$, indicating a hexagonally close-packed ML structure.

Figure 3a shows the appearance of the (10) peak of the NP ML due to 1 ML of hexagonally ordered NPs and its evolution in this run depicted in Figure 2. Figure 3b uses this (10) peak position to track the core−core separation of NPs at the DEG/heptane interface, which is defined as the distance between their surfaces; this separation of the core surfaces for nearest-neighbor NPs attained a steady-state value of 3.44 nm. The dark stars indicate diffuse peaks, while the pink squares indicate sharp peaks.

Then, after more than 2 h of accelerated heptane drying in the cell, SAXS of this sample was performed again with
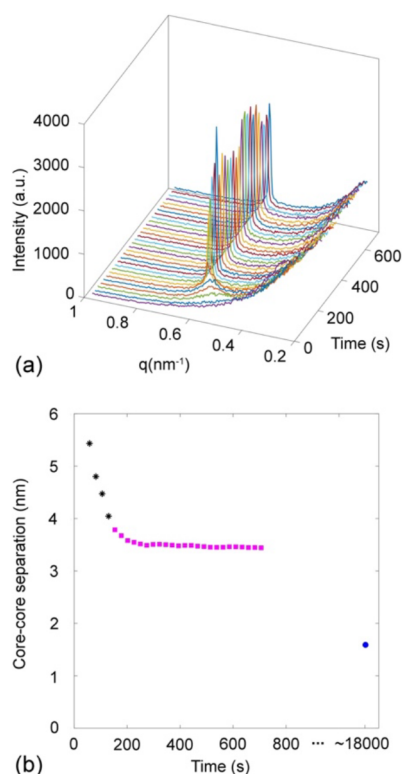
Figure 3. (a) (10) peak shown in Figure 2 at the top of the DEG/heptane interface after 60 μL of 1 ML-equivalent 8.6 nm NP was autodropped onto the heptane reservoir. The (10) peak position is used to track the separation of the nearest-neighbor NP core surfaces over time, as shown in (b). The black stars in (b) indicate the diffuse (10) peaks at the beginning of self-assembly. With more NPs self-assembled, the (10) peaks became sharper and stronger, and the surface separation between the NPs decreased and eventually became stable, shown as pink squares. The blue point shows the NP separation on the DEG/vapor interface, corresponding to the last panel in Figure 2 after the heptane was removed, at 5 h (18 000 s).

heptane no longer present, as seen in Figure 2 at 5 h. The broadened peaks indicate the NPs are still in an ordered ML but no longer a very well-ordered ML at the DEG/vapor interface. The separation of the streaks has increased, indicating that the NP core surface separation has decreased to 1.59 nm, much smaller than the final distance for the DEG/heptane interface. This is in part because the NPs are now at a DEG/vapor interface and not at the DEG/heptane interface; without the heptane there is less shielding of the NP–NP van der Waals attraction. The broadening could also be in part due to wrinkling of this ML due to this area change. After the heptane evaporates, the curvature of the top DEG surface changes from being concave down to flat in this cell designed to flatten the DEG surface. The NPs may become closer with this decrease in surface area if they all remain at the surface. After the heptane layer atop DEG was removed, in a few runs broken short streaks and/or powder rings were seen in addition to these features, respectively indicating the assembly of several ordered layers of NPs and the deposition of 3D polycrystalline arrays of NPs.

3.4. Observed Time Dependence of NP Monolayer Formation for All Runs. For a more general range of conditions, within roughly 10−60 s after drop-casting the dispersion on the heptane reservoir, the SAXS signal at the top

of the meniscus shows vertical streaks that indicate a single ordered, hexagonal ML has formed on the DEG. This is seen for 0.5 ML-equivalent or more of 8.6 nm NPs drop-cast and for 1 ML-equivalent or more of 11.8 nm NPs. (For 8.6 nm NPs, this 0.5 ML-equivalent corresponds to ~1.45 × 0.5−0.72 NP ML coverage of close-packed ordered NPs.) This starts as short and diffuse vertical SAXS streaks appear (Figures 2 and 3), indicating multiple nucleation centers of somewhat ordered 1 ML NP regions that become longer and sharper with time, indicating better and larger ordered regions of 1 ML NPs. The integrated areas of the streaks increase (Figure 4c), reaching their maximum when the streaks are long and sharp. With an increased number of drop-cast NPs, such as 1 ML vs 6 ML-equivalents, the streaks generally become longer and sharper faster, and their integrated areas reach their steady-state values faster, indicating better and faster order.

Before the heptane evaporates (≤~5 h), there is no indication of streaks breaking into several segments, which would indicate the formation of several ordered NP MLs, or streak broadening, which could indicate disordered excess NPs on top of this ordered NP ML. The self-limited formation of 1 NP ML at the DEG/heptane interface was also seen in our optical monitoring experiments.[9] So, drop-cast NPs in excess of 1 ML of close-packed NPs at this interface may remain dispersed in the heptane or migrate to contact lines between the upper and lower menisci and the cell windows and/or walls (see below). At the peripheries of the upper heptane/vapor and the lower DEG/heptane menisci, capillary forces induced by the deformation of the liquid interfaces cause NPs to deposit on the contact lines.[19,20]

Figure 4 shows the signal intensity and peak changes with time, probed at the top of the DEG/heptane interface after the injection of 8.6 and 11.8 nm NPs dispersions for a range of NPs drop-cast, from 0.5 to 12 and 1 to 18 ML-equivalents. Each SAXS run presented in (c)−(f) is fit using a single Gaussian lineshape. Sharp and broad peaks, respectively indicating ordered and disordered NPs, were not seen only for the smallest tested dose drop-cast for the 8.6 and 11.8 nm NPs, 0.2 ML-equivalent; if a close-packed ordered NP ML were present over ~2% or so of the interface area being probed, it would have been noticeable given the measured signal-to-noise ratios. No form factor was also observed because the 5 s integration time was too short for this dilute dispersion. For the 8.6 nm NP run with 0.5 ML-equivalents drop-cast, sharp peaks were seen, but the form factor was rarely seen, likely because the NP concentration was too low. More details about signal analysis, including the integration of the broad SAXS signal due to disordered NPs, is given in Supporting Information Section S9.

In each of the runs shown in Figure 4, the first point usually includes SAXS signal collection during full exposure time, which is after drop-casting and so ends roughly after 8 or 4 s for the longer and shorter exposure times (see Supporting Information Section S10 for more details), except for the first point of the 8.6 nm NPs run with 6 ML-equivalents which ended at t = 2.1 s. Thus, the entire X-ray exposure was before drop-casting. This explains why this first point in Figure 4a of the form factor, without NPs present, is lower than the second point, the first one with NPs present. This also shows that there are significant NPs near this lower meniscus within a few seconds of drop-casting.

Figures 4a and b plot the SAXS NP form factor signal at the top of the DEG/heptane meniscus, integrated along q_x vs q_y
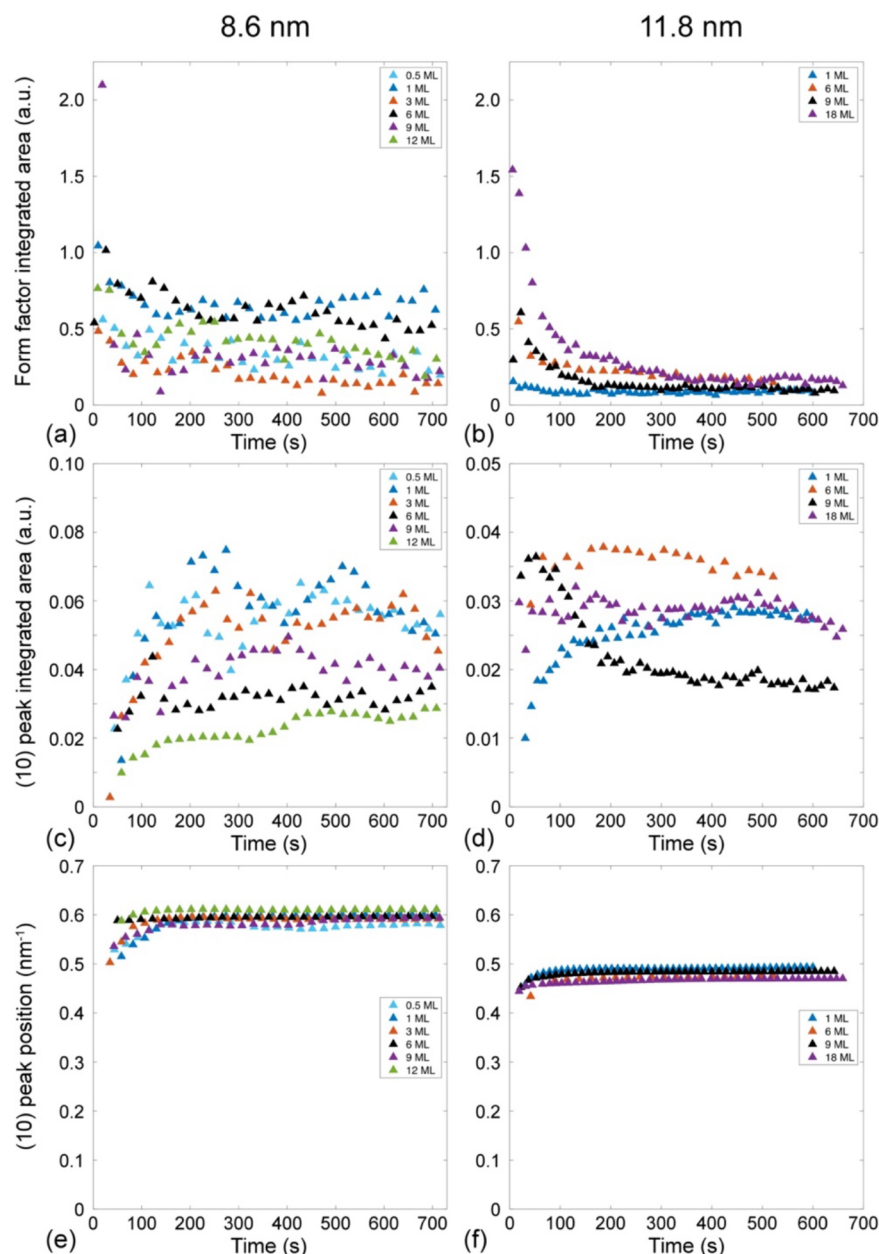
Figure 4. SAXS signal evolution at the DEG/heptane interface after different ML-equivalents of 8.6 nm NPs were autodropped at $t = 0$. Respectively for 8.6 and 11.8 nm NPs, (a) and (b) plot the SAXS NP form factor signal integrated along q_x from -0.0780 to $+0.0780$ nm^{-1} and then fit from $q_y = 1.057$ to 1.598 nm^{-1} for the 8.6 nm NPs and $q_y = 0.745$ to 1.150 nm^{-1} for the 11.8 nm NPs—which indicates the number of disordered NPs the beam can detect in the dispersion and at the interface. (c) and (d) show the area of the (10) peaks, which indicates the number of ordered NPs the beam can detect. (e) and (f) show the peak positions of the (10) peak, which indicates the average short-range separation of the centers of nearest-neighbor NP cores. Each run in (c)−(f) is fit using a single Gaussian lineshape. Data are plotted at the time corresponding to the end of the data collection + reposition period at the DEG/heptane interface.

(Supporting Information Section S9); this is proportional to the sum of the number of randomly dispersed NPs the beam detects in the heptane dispersion and the number of randomly deposited NPs it probes at the DEG/heptane meniscus. This form factor signal was highest at the beginning because the convection after the autoinjection brought the highly concentrated NPs dispersion to the local X-ray detected area, as detailed below. After ∼100 s, SAXS signals from the disordered NPs were relatively uniform, aside from concentration and measurement fluctuations (as discussed below).

Figures 4c and d plot the areas of the (10) peaks, which are proportional to the number of ordered NPs at the interface

that the beam probes, with the NPs likely in large clusters. The peak areas increased during the formation of the ordered ML. The time needed to approach the maximum values, with the ML almost fully packed, is generally shorter when more NPs were drop-cast, from ∼220 s for 1 ML-equivalent to ∼90 s for 12 ML-equivalents for 8.6 nm NPs. Figures 4e and f plot the peak position of the (10) peak, which provides the average short-range core−core distance. Supporting Information Figure S11 presents these data in terms of the areal densities of NPs. The peak widths are presented in Supporting Information Figure S12. For most, but not all, runs with 8.6 nm NPs, the final widths are attained within ∼100 s. For all
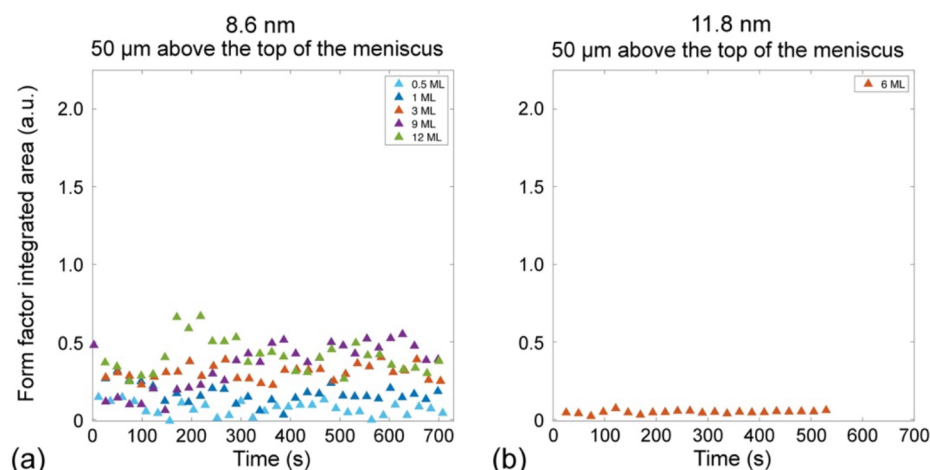
Figure 5. SAXS, integrated over the form factor, taken 50 µm above the DEG/heptane meniscus, with the same conditions as in Figure 4 for (a) all of the 8.6 nm NP runs (except for 6-ML equivalents) and (b) the one 11.8 nm NP run with the longer, 5 s data acquisition time (6 ML-equivalents), for which data at this position were taken. The same a.u. (arbitrary units) are used as in Figures 4a and b.

runs with 11.8 nm NPs, this evolution is quicker and more uniform; the final widths are attained within 50 s. Perhaps the larger van der Waals interactions between these larger NPs and between them and the interface leads to the quicker evolution to high-quality ordered arrays of NPs.

Figure 5 shows representative SAXS data taken just above the DEG/heptane interface, with more details given in Supporting Information Section S14. Only the integrated form factor data are plotted because no sharp peaks due to ordered NPs were seen, as is expected. This figure does not show the decrease in form factor at the top of this interface that is seen up to 100 s in Figures 4a and b, after which it is very roughly the same level as that above the meniscus. It is possible that this is due to a very early areal density of disordered NPs on the meniscus, and this decrease occurs as the NPs order; transport of more NPs from the dispersion to the interface may also be occurring in this time frame.

There is less scatter in the 8.6 nm NP runs, and so better conclusions can be drawn from them than from most of those with 11.8 nm NPs because all of the former runs had longer integration times and less X-ray background. Several consistent conclusions can be drawn from Figures 4a, c, and e and Figure 5a. The NPs mix rapidly and arrive very quickly, within ~20 s, in the NP dispersion just above the DEG/heptane meniscus (Figure 5). The areas of the sharp (10) peaks increase in ~100 s to their steady-state values due to close packing and hexagonal order (Figure 4c). In the integrated form factors measured at the DEG/heptane meniscus, signals are high within ~20 s of drop-casting and then decrease to approximately steady-state values within 100 s. Since these are due to disordered NPs and could include NPs in the dispersion and disordered NPs at the interface, very soon after drop-casting there are many disordered NPs at the interface, and the signal decreases over ~100 s as these NPs order and the area of the sharp ordered peak increases over the same time scale. There is a decrease of the nearest-neighbor distance in the ordered NPs, seen by the increase in Figure 4e over the first ~100 s, and this is consistent with the increase of the sharp peak areas and the decrease in the integrated form factors attributed to disordered NPs at the interface. Since the nearest-neighbor NP distances are larger for disordered NPs than for ordered NPs, their NP areal densities are smaller, so

there is likely some transport of NPs from the dispersion to the interface during this first ~100 s.

However, the nearest-neighbor distances begin at a value very near the steady-state one and evolve to its steady-state value in ~100 s, as deduced from Figure 4e. If the entire meniscus were covered with ordered NPs very early, this would suggest that the number of ordered NPs at the meniscus would be near its maximum very much earlier than ~100 s. This is not consistent with the slower increase of the area of the ordered peak with time, which is presumably proportional to the area of the patches of ordered NPs being measured. This suggests that the fraction of surface covered with ordered arrays of NPs is continuously increasing over the first 100 s.

The integrated areas of the form factors measured at the interface (Figure 4a) decrease to approximately the values measured above the interface (Figure 5a) as the 8.6 nm NPs at the interface order. This decrease is also seen for most of the 11.8 nm NP runs in Figure 4b; however, the comparison is best for the 6 ML-equivalent run, with its longer integration time and comparison measurement above the interface, shown in Figure 5b. This early decrease makes sense because even when the beam is positioned at the interface, as we will see, ~ 90% of the volume probed by the X-ray beam is from regions of the NP dispersion. (NPs in the dispersion are measured over the entire 11.58 mm path length of the X-ray beam above it (Supporting Information Section S6).) Over the 11.56 mm path length at the interface, only NPs in the dispersion are probed by the entire beam, which occurs over 11.56 mm − 3.26 mm = 8.30 mm, 3.26 mm being the length of the meniscus being probed there (Supporting Information Section S6). Across this 3.26 mm long region, between 50% and 100% of the beam volume probes the dispersion, from the center to the edges of the probed meniscus; over the 11.56 mm path length, ~90% of the volume probes only the dispersion (Section S6).

The very roughly 40%−90% decrease in signal in Figure 4a over the first 100 s or so would suggest that initially the number of disordered NPs being probed on the meniscus is roughly 0.7−9 times the number of NPs being probed in the dispersion. (The background signal has been subtracted.) The number of NPs being probed *at the meniscus* is $n_{probed, meniscus} = \rho_{disordered}A$, where $\rho_{disordered}$ is the areal density of disordered
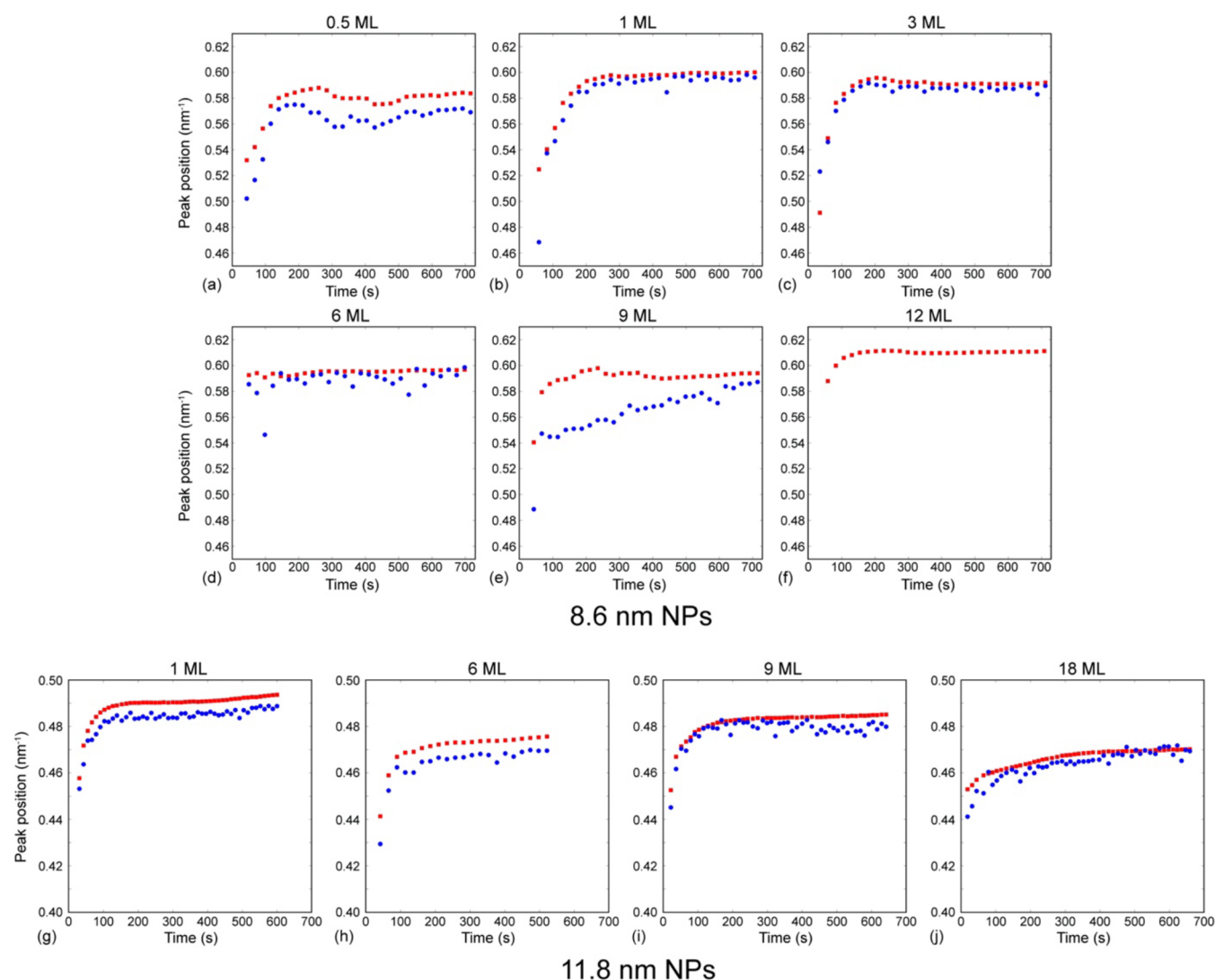
Figure 6. Ordered peak positions for all the NP SAXS runs, using two Gaussian lineshapes for the fit. Those of the sharper and usually larger peaks are given by the red squares and those of the broader and usually weaker peaks by the blue circles. The ordinate units are the same in each plot.

NPs at the meniscus at the time and A is the meniscus area probed, ~200 μm × 3.26 mm. (The arc length and length probed are essentially the same here; see Supporting Information Section S6.) The number of NPs being probed *in the dispersion* is $n_{\text{probed, dispersion}} = \xi n_{\text{rem disp}}$, where ξ is the ratio of the volumes of the X-ray beam probing the dispersion and the heptane dispersion layer, and $n_{\text{rem disp}}$ is the number of NPs remaining in the dispersion. ξ is (50 μm × 200 μm × 11.56 mm × 0.90)/(1.06 mL), and $n_{\text{rem disp}} = N_{\text{ML rem disp}} \rho_{\text{ordered}} S$, where $N_{\text{ML rem disp}}$ is the number of ML-equivalents remaining in the dispersion, as calibrated in the Petri dish, ρ_{ordered} is the areal density of close-packed ordered NPs, and S is the surface area of the calibration meniscus, ~6.7 cm^2 (Supporting Information Section S3). So, the estimated ratio of NPs probed at the meniscus to that in the dispersion is

$$\frac{n_{\text{probed, meniscus}}}{n_{\text{probed, dispersion}}} \sim \frac{\rho_{\text{disordered}} A}{\xi N_{\text{ML rem disp}} \rho_{\text{ordered}} S} \sim \frac{9.9}{N_{\text{ML rem disp}}}$$

$$\times \frac{\rho_{\text{disordered}}}{\rho_{\text{ordered}}}$$

The last factor is at most ~0.9 for disordered NPs fully covering the meniscus (see below),[21] so the measured ratio of ~0.7−9 suggests that very early during the first 100 s, very roughly 8−100% of the meniscus is covered with disordered 8.6 nm NPs (for 1 ML-equivalent of NPs remaining in the dispersion), which is a significant amount. The data in Figures 4b and 5b also suggest quite sizable early coverage of this interface with disordered 11.8 nm NPs.

If the SAXS signals for disordered dispersed NPs and disordered NPs at an interface were in fact different, perhaps with different signatures vs q_x and q_y, this would be noticeable, but as expected the data showed this was not the case.

If 1 ML-equivalent of NPs forms at the DEG/heptane interface when at least these number of NPs have been drop-cast, one would expect the remaining NPs would remain in the dispersion in steady state and the form factor signals would increase linearly with the number of drop-cast NP ML-equivalents increasing. This is seen in Figure 5a but not in Figure 4a because of the uncertainties and sensitivities in the measurements (see below in Section 3.6). The SAXS signal intensity at the top of the DEG/heptane meniscus is sensitive to the beam location due to the strong X-ray absorption of
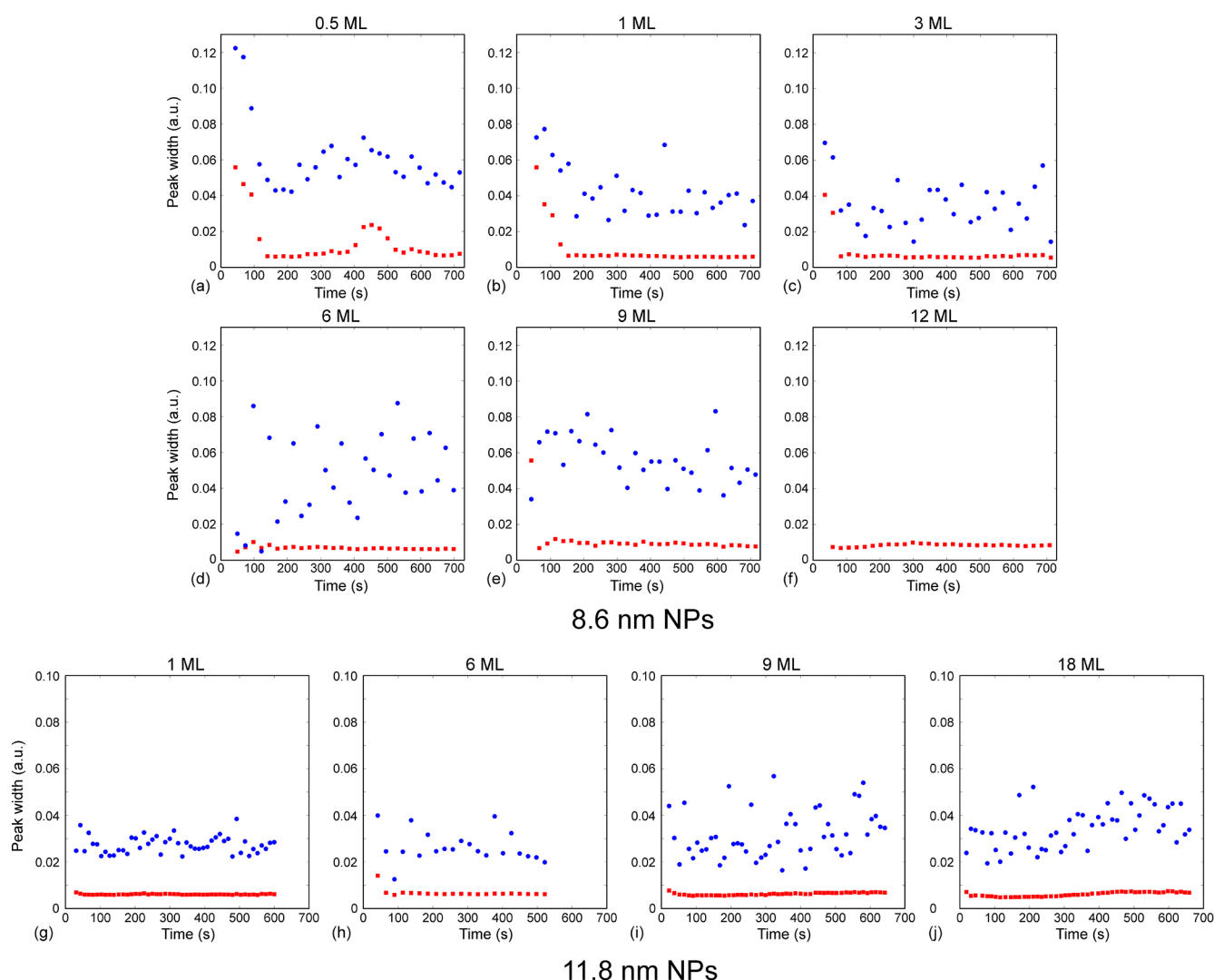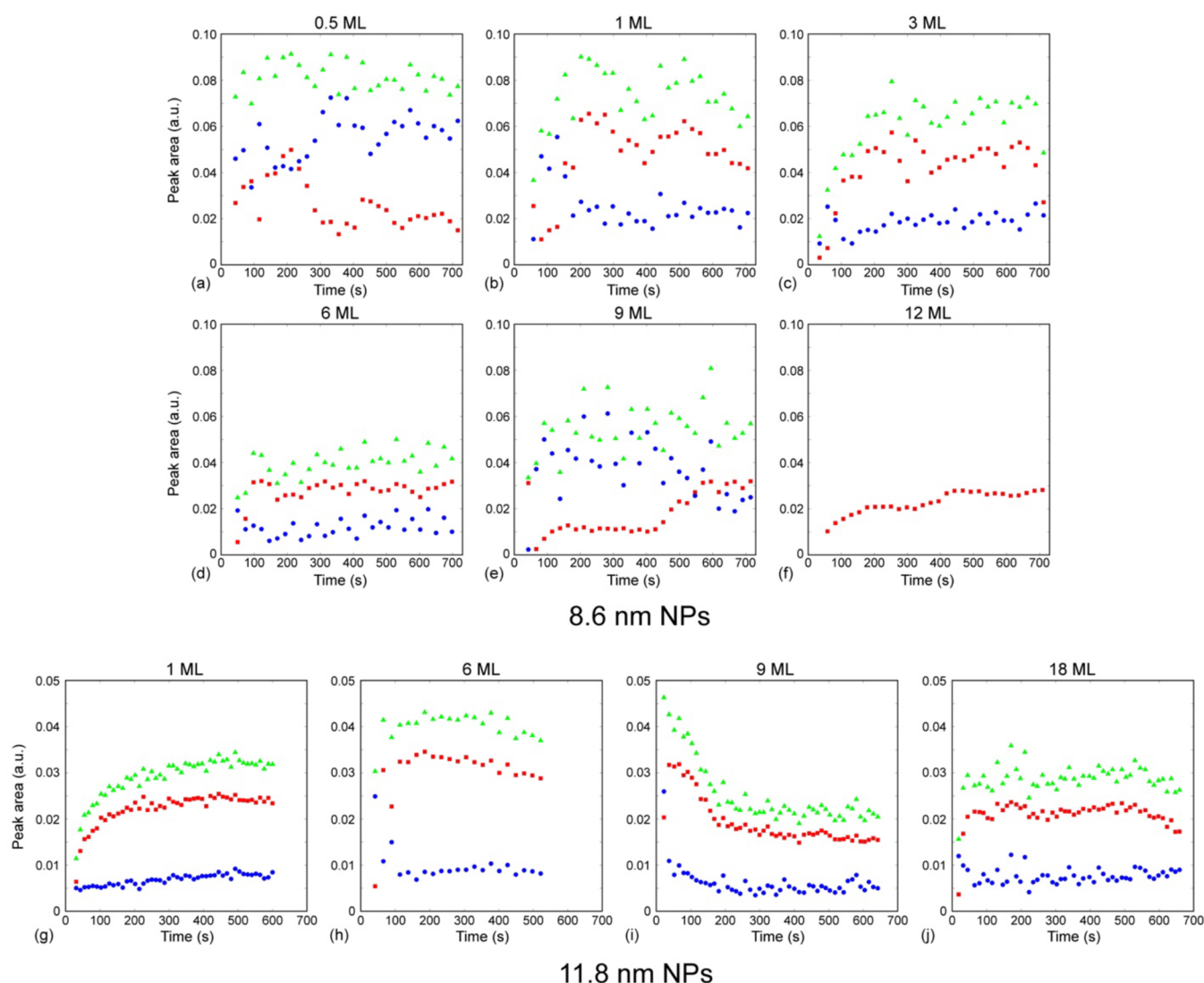
Figure 7. Ordered peak widths for all the NP SAXS runs, using two Gaussian lineshapes for the fit. Those of the sharper and usually larger peaks are given by the red squares and those of the broader and usually weaker peaks by the blue circles. The ordinate units are the same in each plot.

DEG. So, the SAXS signal intensities of both coherent and incoherent signals at the top of the DEG/heptane meniscus are more useful in indicating trends in time during a single run than in comparing different runs. However, the signal from above the top of the DEG/heptane meniscus is much less sensitive to beam location, and so it can be used to compare the integrated SAXS form factor signals between runs. This is also likely because excess NPs have been deposited at the contact lines at the DEG/heptane and heptane/vapor menisci and the cell windows and walls (Supporting Information Figure S15), as in ref 19. The evaporation of the heptane and the receding contact lines can account for deposits at the heptane/vapor contact lines. The curvature and possibly convection can drive the particles to the contact lines of both menisci. There can be recirculation flows as the heptane phase evaporates and the heptane film is "squeezed."

3.5. Multiple Sharp SAXS Peaks and Types of Ordering at Different Places at the DEG/Heptane Interface. The data describing the (10) peaks in Figures 4c−f were obtained using a single Gaussian lineshape. In most cases there was only a single ordered NP peak, or that peak was very dominant. The peak widths for the 0.5 and 9 ML-

equivalent runs for 8.6 nm NPs presented in Supporting Information Figure S12 showed unusual behavior, and this was resolved by fitting the data for 8.6 nm NPs with two Gaussian peaks. The parameters from all of these two-lineshape fits for both sets of NPs are shown in Figures 6, 7, and 8, with sample fits and more information given in Supporting Information Figures S13 and S14. For 8.6 nm NPs, only one very sharp peak was needed to fit the 12 ML-equivalent run, showing that all probed regions consisted of close-packed, well-ordered NPs. For the 1, 3, and 6 ML-equivalents runs, one peak, the "sharper" one, was very narrow, stronger, and at a larger q vector, the major peak in these cases, indicating larger areas probed of close-packed, well-ordered NPs, with the "smallest possible" NP separations. The other peak, the "broader" one, was significantly broader, weaker, and at a somewhat smaller q vector, the minor peak in these cases, indicating the probing of much smaller areas of less well-ordered NPs with larger NP separations. These separate regions or sets of large clusters of similar separate regions form within 100 s and do not evolve much later. For 9 ML-equivalents, the sharper peak is initially the weaker one and becomes stronger while the broader peak becomes smaller, and at ∼700 s the sharper peak is the larger

Figure 8. Ordered peak areas for all the NP SAXS runs, using two Gaussian lineshapes for the fit. Those of the sharper and usually larger peaks are given by the red squares and those of the broader and usually weaker peaks by the blue circles, and the sum of these peaks is given by the green triangles. The ordinate units are the same in each plot. The same a.u. (arbitrary units) are used as in Figures 4c and d.

of the two, so there is evolution of the two regions. This different dependence for this run is thought to be due to run-to-run variations. Also, the "disturbance" in peak width near 450 s for the 0.5 ML-equivalents run in Figure 7 is thought to be a momentary variation and not to be significant.

The 0.5 ML-equivalent run corresponds to drop-casting enough 8.6 nm NPs to form ∼0.72 ML of close-packed NPs at the DEG/heptane interface. Two (10) peaks are still seen, and they both form within ∼100 s, but they are quite different. The sharper peak in this case is always the weaker of the two, and in fact its area decreases with time, while that of the broader peak increases with time. The difference in the steady-state peak positions of the broader peak relative to the sharper one is ∼2.6%, which is much more than that in the other runs and corresponds to a core surface separation within the NP cluster that is larger in the more loosely packed structure by ∼0.3 nm (∼4.1 vs ∼3.8 nm) (Figure 6). Therefore, the steady-state areal packing density associated with regions leading to the broader peak is ∼5.2% smaller than that for the sharper one, which is associated with close packing, and this percentage difference is the largest that is seen for these runs. The areal packing

fraction for ordered close packing of identical hard cylinders or spheres in 2D is ∼0.907. That for random close packing (RCP) is ∼0.82−0.84;[21] above this fraction there is some order, and the larger it is, the higher the degree of order. So, the areal density for RCP is ∼7−10% smaller than that for ordered close packing. If the 8.6 nm NPs, with core and ligands, are treated as hard spheres, the relative areal density for the loosely ordered state, only ∼5.2% smaller than that for close packing, is larger than that expected for RCP. This is as expected and is, of course, consistent with their SAXS patterns. The small particle core diameter dispersion of ∼10% (standard deviation/median) here affects these conclusions little.

So, these close-packed NP regions form within 100 s, but for small doses of NPs they evolve to less well-ordered regions of ordered NPs, maybe because they are less stable when there are not enough NPs at the interface to form a close-packed NP ML everywhere at the DEG/heptane meniscus. The close-packed region is stable after drop-casting more than enough NPs to cover the entire meniscus. At the steady state of the runs for 8.6 nm NP runs with 1, 3, and 6 ML-equivalents and 11.8 nm NPs with 9 and 18 ML-equivalents, the broader and

sharper peaks are very close, so their NP–NP distances are almost the same and they are both hexagonally close packed. The width of the broader peak may be due to small grains of NPs arising from defects during assembly or nucleation sites. This would be expected when NPs cover the entire interface. When the broader and sharper peaks are further apart, the broader peaks may represent regions with smaller clusters or assemblies of ordered NPs that are not close packed, where the NPs are further apart and not locked in place relative to each other as in the close-packed regions. The wider range of inter-NP distances in a small NP cluster and the range of sizes of small clusters, which causes an even larger variation of inter-NP distances, cause the larger widths of these assemblies. The prevalence of these smaller clusters would be expected particularly when there are not enough NPs to cover the entire interface.

Two peaks are also expected for distorted hexagonal-like order because of the two nearest-neighbor inter-NP distances.[22] However, given that these double peaks do not have similar widths, as would be expected from that pattern, and their peak locations are not what would have been expected, this distorted hexagon pattern does not appear to be important here.

Two peaks also appear in the first-order SAXS region for 11.8 nm NPs. The broader (10) peaks for these NPs are nearer to the sharper peaks and so are closer in peak position and relatively weaker, i.e., with smaller peak areas, compared to the corresponding SAXS peaks in the 8.6 nm NP runs. This means that the 11.8 nm NPs formed MLs with better order and likely larger area clusters than those with 8.6 nm NPs. This makes sense because the larger NPs have stronger van der Waals NP–NP attraction energies. This is another reason to associate the broader (10) peaks with smaller clusters of NPs.

3.6. Sensitivity of the Numbers of NPs Being Probed to Experimental Conditions. The SAXS intensity is proportional to the numbers of NPs being probed and the X-ray beam strength. Precise quantitative comparison of the integrated sharp peaks and of the form factor intensities is challenging because of (a) variations in vertical alignment at the meniscus within a run after drop-casting vs time due to differing numbers of NPs probed both on the surface and in the dispersion and different X-ray absorption in the solvents for slightly different beam locations, and (b) variations in beam intensity during a day in a run and between different visits to the beam source. This is addressed briefly here and in more detail in Supporting Information Sections S3 and S6. There are also systematic random uncertainties in determining and delivering the number of NPs corresponding to the number associated with a given number of close-packed NP MLs at the meniscus.

Supporting Information Figures S5–S7 can be used to estimate the uncertainty in the relative vertical location of each of the beam positions relative to the DEG/heptane meniscus due to backlash and other alignment uncertainties. "At" the top of the DEG/heptane meniscus means the center of the beam can range from 25 μm below to above the top of the interface with the middle of this being the target. This could lead to variations in the consecutive measurements of the areas of the sharp SAXS peaks due to ordered NPs at this interface and of the broad underlying SAXS background due to any disordered NPs at the interface, for two reasons: (1) the beam can intersect and so probe the interface over different areas and across different path lengths in the dispersion over this range of

locations; and (2) the path length of the beam within the DEG can vary, and this affects the intensity of all detected SAXS signals because DEG absorbs X-rays more strongly than does heptane. This can lead to sizable scatter in the areas of integrated intensities that is not present in the SAXS peak locations, but magnitudes of the areas still provide some useful information. There are also systematic and random errors in the quantitative dosing of NPs.

The uncertainty in vertical alignment is thought to be better than 50 μm because sharp SAXS peaks are never seen when the beam is supposed to be above the interface and are always seen when the beam should be at the interface, along with the beam reflection signature from the top of the interface.

When the beam is at the top of a meniscus with close-packed, ordered NPs, $\sim 5.05 \times 10^9$ of 8.6 nm NPs and $\sim 3.29 \times 10^9$ of 11.8 nm NPs are being probed at the DEG/heptane interface. When the beam is "just below" the meniscus, a larger meniscus area is probed (~ 0.85 vs ~ 0.65 mm^2) and so more NPs are probed: $\sim 6.61 \times 10^9$ of 8.6 nm NPs and $\sim 4.30 \times 10^9$ of 11.8 nm NPs. This illustrates one factor in the measurement uncertainty, as is detailed in Section S3. Section S3 also gives estimates of the numbers of NPs probed at the DEG/vapor interface and in the NP dispersion.

This accuracy of alignment leads to different degrees of X-ray beam transmission and so very different detected SAXS signals due to absorption of the incident and scattered beams because of the different X-ray absorption coefficients in heptane and DEG. For the beam positioned totally in the heptane, on top of the DEG/heptane meniscus (Supporting Information Section S6), $\sim 52.3\%$ of the beam is transmitted; 25 μm lower "at" the top of the meniscus, $\sim 46.8\%$ is transmitted; and with its top positioned at the top of the DEG meniscus, $\sim 37.8\%$ is transmitted.

3.7. Transport of NPs after Drop-casting. The time dependence of the formation of the ordered NP ML at the DEG/heptane interface depends on the (1) mechanism of transport of NPs from the drop-casting site to this liquid interface, which entails the evolution of the drop, including it mixing with the existing heptane reservoir, (2) NP adhesion at this DEG/heptane interface, (3) the evolution of disordered NPs at this interface to an ordered, close-packed ML, even as more NPs from the dispersion impinge at the interface, and (4) changes that occur when the heptane layer evaporates. This first step critically depends on the collision of the drop with the top surface during drop-casting. Points 3 and 4 were discussed above. Points 1 and 2 are discussed now.

The NP dispersion drop was delivered from the end of a capillary tube with a 0.79 mm inner diameter located at height $h = 2$ mm above the center of heptane/vapor interface. The liquid volume released is 60 μL, which corresponds to a single spherical drop with radius $r = 2.5$ mm. Based on the mass density[23] $\rho = 684$ kg/m^3, surface tension[23] $\gamma = 20.14$ mN/m, and viscosity[24] $\eta = 3.8 \times 10^{-4}$ Pa·s of the heptane phase, the delivered drop is characterized by a finite Bond number $Bo = \rho g r^2 / \gamma \simeq 2$, determined by the ratio of gravitational and capillary forces, and a small Ohnesorge number $Oh = \eta / \sqrt{\rho \gamma r} \simeq 2 \times 10^{-3}$, determined by the ratio of viscous to inertial and capillary forces. Under such conditions the NP dispersion droplet is expected to fully coalesce with the heptane interface in a characteristic time $\tau = \sqrt{2r/g} \simeq 0.02$ s determined by the ratio of inertia and gravitational forces.[25,26] The corresponding characteristic speed for the coalescence

process is $v = 2r/\tau \simeq 0.2$ m/s, which gives a large Reynolds number $Re = \rho v r/\eta \sim 1000$. So, convective effects dominate the fluid flow, and rapid mixing occurs after the NP dispersion droplet coalesces with the heptane film. These general conclusions remain valid when the NP dispersion volume breaks into two to three droplets during the ~3 s injection time. For smaller droplets with $Bo < 1$, the ratio of capillary and inertial forces determines a coalescence speed $v = \sqrt{\gamma/2\rho r} \simeq 0.08$, and the corresponding Reynolds number remains much larger than unity.

The Peclet number characterizing the transport of NPs in the heptane after coalescence of the drop is $Pe = vR/D$, where R is the radius of the spherical iron oxide NP and $D = k_B T/6\pi\eta R$ is the NP diffusivity. For NPs with $R = 4.3$ and 5.9 nm, the Peclet number is $Pe = 7$ and 13, respectively, which indicates that advective NP transport dominates over diffusion shortly after deposition. The shortest possible time to transit the thickness of the heptane reservoir ($h_e \simeq 0.5$ mm) is $\sim h_e/v = 2.5$ ms, while the decay time for the flow generated after the droplet coalescence is $\sim \rho r^2/\eta = 10$ s, which is consistent with the early appearance of NPs near or at the DEG/heptane interface (Figure 4). For reference, the time for the NPs to diffusively cross the thickness of the heptane reservoir is $h_e^2/2D$, which is on the order of 1000 s. Based on the temporal evolution of the SAXS form factors (Figure 4a), the time scale for NP transport to the DEG/heptane interface appears to range from 2 to 20 s, which is consistent with NP transport dominated by advection.

Additional factors influencing the temporal evolution of the SAXS form factors are the finite times required for NPs to adsorb and attach irreversibly to the DEG/heptane interface. While the ratio of driving capillary forces and viscous damping gives extremely short times $T_d \sim 0.1$ ns for NP adhesion to a liquid/liquid interface, recent work on single particles indicates that energy barriers induced by surface defects or grafted polymer chains can produce unexpectedly long adhesion times, larger than several seconds.[27−29] For example, large energy barriers of $\Delta U = 25-30\ k_B T$, as produced by defect areas ~4−6 nm^2, and the associated slow thermally activated processes could result in adsorption times $T_d \sim \exp(\Delta U/k_B T) \sim 10-1000$ s for a single NP.[28] Similarly, slow thermally activated processes govern the structural relaxation of the NP assembly at the interface, which could result in long relaxation times ~10−1000 s.

The transport of drop-cast NPs was explored further experimentally by varying the thickness of the heptane reservoir by drop-casting a 60 μL dispersion containing 6 ML-equivalents of 11.8 nm NPs on top of predeposited 0.5, 1.0, 2.0, and 4.0 mL heptane reservoirs on 2.0 mL of DEG, and then followed by using SAXS at and near the top of the meniscus, as detailed in the Supporting Information Section S16 and Figures S16−S18. These runs were all performed during the same visit to NSLS-II but a different visit than those used to obtain the data in Figures 1−8. (This 1.0 mL run was in addition to those performed during the base-case studies of earlier visits.) Before drop-casting the dispersion, the thickness of the heptane layer in the center of the meniscus was measured to be 0, 0.55 (as opposed to the 0.50 mm measured in the earlier 1.0 mL run), 2.10, and 4.25 mm, by using X-ray scanning (Supporting Information Figure S19); for the last three cases the thickness increases by ~0.1 mm after drop-casting the dispersion. This thickness was 0 mm for the 0.5 mL

heptane reservoir on DEG (Figure S19a) because the lower, DEG/heptane interface was still concave down and the upper, heptane/vapor interface was still concave up, and there was not enough heptane to cover the top of the DEG layer so heptane resided only in the periphery, as depicted in Supporting Information Figure S20. The intensity of the form factor decreased to a steady-state value within a few minutes after drop-casting, showing that the NPs were then dispersed fairly uniformly in the heptane layer. This time increased from ~1.8, ~2.6, ~7.5, and ~9.5 min, for the 0.5, 1.0, 2.0, and 4.0 mL runs, respectively (Supporting Information Figure S16). However, the time dependence of the evolution of the (10) NP peak at the DEG/heptane interface varied similarly for each of these reservoir volumes, with generally the same steady-state peak intensities and separations—and so the above observations about NP transport are not changed.

For the 0.5 mL run, X-ray transmission before drop-casting the NP dispersion indicated no detectable heptane layer in the middle of the DEG (Supporting Information Figures S19 and S20), and so at the top interface there was DEG/vapor and not DEG/heptane; this is expected given the volume and the surface tensions of each liquid. However, the (10) peaks for the ordered NP ML, and so the NP separations, were the same as for the other runs where the ML was clearly at a DEG/heptane interface, ~3.3 nm separation between the surfaces of the cores of the nearest-neighbor NP, and not those expected for those at a DEG/vapor interface, as in Figure 3 after heptane evaporation and for drop-casting the NP dispersion directly on DEG (followed by the rapid evaporation of heptane), ~1.9 nm separation. This suggests that there was still a very thin heptane wetting layer atop the DEG in the middle.

3.8. Comparison Study: Drop-casting Directly on the DEG Layer. When 1 ML-equivalent or more of 11.8 nm iron oxide NPs in heptane are directly dropcast on DEG (here, as in ref 5), after the relatively rapid heptane evaporation (~5 min) SAXS at the top of the meniscus shows vertical streaks that indicates a single ordered, hexagonal NP ML forms on the DEG (Supporting Information Section S17, Figure S21a). These signals indicate approximately the same NP separation as after heptane dispersion deposition on a heptane reservoir which then dries (Supporting Information Figure S21b), but the latter have broader peaks. Excess NPs forming a disordered structure on top of it may be indicated by the broader streaks when more than a single ML-equivalent is drop-cast. There is no indication of breaking of each streak into vertical segments, which would indicate multiple ordered MLs.

4. CONCLUSIONS

Spatial and temporal SAXS scans show that 8.6 and 11.8 nm iron oxide NPs in heptane drop-cast on top of a heptane layer atop a DEG layer are trapped at the DEG/heptane interface to generally form a single ordered, hexagonal close-packed ML, and this occurs long before the heptane evaporates (and this is in contrast to the conclusions of our earlier studies). The van der Waals binding between the NPs in the heptane is too weak to form multiple layers, even given a template of ordered NPs at the DEG/heptane interface, which is not surprising given that it disperses well in this liquid. Excess drop-cast NPs remain dispersed in the heptane or migrate to the cell periphery even when many ML-equivalents of NPs are drop-cast. These SAXS observations of self-limited NP ML formation at the DEG/heptane interface are consistent with

those using the less direct method of real-time optical reflection monitoring of that interface.

NPs were drop-cast here on a pre-existing heptane layer here to try to resolve the transport of NPs to the DEG/heptane interface. However, NPs are seen to be present at and near this meniscus much faster than expected by considering only the diffusion of NPs from the drop-cast site to this liquid/liquid interface, so there is rapid mixing of the NPs throughout the dispersion even with "gentle" drop-casting. So, NP transport is not the rate-limiting step in NP assembly at the DEG/heptane interface.

The formation of the ordered NP ML occurs within 100 s of drop-casting. Over the same time, there is a decrease in the disordered NPs measured across the X-ray path at the top of the meniscus that is not seen just above it, so there are disordered NPs at the DEG/heptane interface while the ordered layer is forming. Over this time, the fraction of the interface covered with ordered NPs can be continuously increasing.

At the DEG/heptane interface there is evidence of regions where the ordered NPs are not close-packed, but this is over much smaller areas than the close-packed regions, except when there are not enough NPs to cover the entire interface. So, after drop-casting, NPs can exist at the DEG/heptane interface in three ways: (1) disordered, apparently only soon after drop-casting, (2) ordered but not close-packed, the minority ordered phase in steady state, except it is dominant when sub-ML-equivalents of NPs are drop-cast, perhaps because they are small clusters of ordered NPs, and (3) ordered and close-packed, the usual dominant phase in steady state.

After the heptane evaporates, an ordered NP ML remains at the DEG/vapor interface, though with smaller NP−NP separation, as expected due to less van der Waals shielding caused by the upper medium in the interface.

Scans of X-ray beam transmission, horizontally at different vertical positions in multiple liquid systems, combined with SAXS characterization of NPs dispersed in these liquids and at and near the liquid interfaces, taken at different times, can help give a clear picture of NP assembly. This method could be valuable in future studies of interfacial assembly.

ASSOCIATED CONTENT

Ⓢ Supporting Information

The Supporting Information is available free of charge at https://pubs.acs.org/doi/10.1021/acs.jpcc.0c07024.

Complementary information regarding the (1) SAXS cell, (2) X-ray beam path and measurement, (3) calibration of the interfacial coverage of nanoparticles and the number being probed, (4) X-ray beam blocking, (5) DEG/heptane meniscus shape and X-ray transmission (without NPs), (6) X-ray beam height relative to the meniscus, (7) NP form factors, (8) SAXS below the meniscus, (9) more details about SAXS data analysis, (10) time of the first collected SAXS data at the DEG/heptane interface relative to drop-casting, (11) areal density of the ordered NPs at the DEG/heptane meniscus vs time, (12) widths of the ordered SAXS peaks at the DEG/heptane meniscus vs time, (13) fitting the ordered SAXS peaks at the DEG/heptane meniscus with two Gaussian lineshapes, (14) SAXS measurements above the DEG/heptane meniscus, (15) contact lines, (16) SAXS after NP drop-casting on different heptane reservoirs, atop DEG, and (17) direct drop-casting of NPs on DEG (PDF)

AUTHOR INFORMATION

Corresponding Author

Irving P. Herman − *Department of Applied Physics and Applied Mathematics, Columbia University, New York, New York 10027, United States;* ⊙ orcid.org/0000-0001-8492-6000; Email: iph1@columbia.edu

Authors

Jiayang Hu − *Department of Applied Physics and Applied Mathematics, Columbia University, New York, New York 10027, United States;* ⊙ orcid.org/0000-0001-6707-1549

Evan W. C. Spotte-Smith − *Department of Applied Physics and Applied Mathematics, Columbia University, New York, New York 10027, United States;* ⊙ orcid.org/0000-0003-1554-197X

Brady Pan − *Department of Applied Physics and Applied Mathematics, Columbia University, New York, New York 10027, United States;* ⊙ orcid.org/0000-0002-9690-1270

Roy J. Garcia − *Department of Applied Physics and Applied Mathematics, Columbia University, New York, New York 10027, United States;* ⊙ orcid.org/0000-0003-0861-873X

Carlos Colosqui − *Department of Mechanical Engineering and Department of Applied Mathematics and Statistics, Stony Brook University, Stony Brook, New York 11794, United States;* ⊙ orcid.org/0000-0002-7215-512X

Complete contact information is available at:
https://pubs.acs.org/10.1021/acs.jpcc.0c07024

Author Contributions

The manuscript was written through contributions of all authors. All authors have given approval to the final version of the manuscript.

Notes

The authors declare no competing financial interest.

REFERENCES

(1) Dong, A.; Ye, X.; Chen, J.; Murray, C. B. Two-Dimensional Binary and Ternary Nanocrystal Superlattices: The Case of Monolayers and Bilayers. *Nano Lett.* **2011**, *11*, 1804−1809.

(2) Asbahi, M.; Lim, K. T.; Wang, F.; Duan, H.; Thiyagarajah, N.; Ng, V.; Yang, J. K. Directed Self-Assembly of Densely Packed Gold Nanoparticles. *Langmuir* **2012**, *28*, 16782−16787.

(3) Zhang, D.; Hu, J.; Kennedy, K. M.; Herman, I. P. Forming Nanoparticle Monolayers at Liquid−Air Interfaces by Using Miscible Liquids. *Langmuir* **2016**, *32*, 8467−8472.

(4) Aleksandrovic, V.; Greshnykh, D.; Randjelovic, I.; Fromsdorf, A.; Kornowski, A.; Roth, S. V.; Klinke, C.; Weller, H. Preparation and Electrical Properties of Cobalt-Platinum Nanoparticle Monolayers Deposited by the Langmuir-Blodgett Technique. *ACS Nano* **2008**, *2*, 1123−1130.

(5) Zhang, D.; Lu, C.; Hu, J.; Lee, S. W.; Ye, F.; Herman, I. P. Small Angle X-Ray Scattering of Iron Oxide Nanoparticle Monolayers Formed on a Liquid Surface. *J. Phys. Chem. C* **2015**, *119*, 10727−10733.

(6) Pieranski, P. Two-Dimensional Interfacial Colloidal Crystals. *Phys. Rev. Lett.* **1980**, *45*, 569.

(7) Fortini, A. Clustering and Gelation of Hard Spheres Induced by the Pickering Effect. *Phys. Rev. E* **2012**, *85*, 040401.

(8) Cheung, D. L.; Bon, S. A. Interaction of Nanoparticles with Ideal Liquid-Liquid Interfaces. *Phys. Rev. Lett.* **2009**, *102*, 066103.

(9) Hu, J.; Pan, B.; Makihara, T.; Garcia, R. D.; Herman, I. P. Brewster Angle Optical Reflection Observation of Self-Limiting Nanoparticle Monolayer Self-Assembly at a Liquid/Liquid Interface. *AIP Adv.* **2019**, *9*, 065022.

(10) Lu, C.; Zhang, D.; van der Zande, A.; Kim, P.; Herman, I. P. Electronic Transport in Nanoparticle Monolayers Sandwiched between Graphene Electrodes. *Nanoscale* **2014**, *6*, 14158−14162.

(11) Zhang, D.; Wang, D. Z.-R.; Creswell, R.; Lu, C.; Liou, J.; Herman, I. P. Passivation of CdSe Quantum Dots by Graphene and MoS_2 Monolayer Encapsulation. *Chem. Mater.* **2015**, *27*, 5032−5039.

(12) Albrecht, M.; Hu, G.; Guhr, I. L.; Ulbrich, T. C.; Boneberg, J.; Leiderer, P.; Schatz, G. Magnetic Multilayers on Nanospheres. *Nat. Mater.* **2005**, *4*, 203−206.

(13) Fan, J. A.; Wu, C.; Bao, K.; Bao, J.; Bardhan, R.; Halas, N. J.; Manoharan, V. N.; Nordlander, P.; Shvets, G.; Capasso, F. Self-Assembled Plasmonic Nanoparticle Clusters. *Science* **2010**, *328*, 1135−1138.

(14) Hyeon, T.; Lee, S. S.; Park, J.; Chung, Y.; Na, H. B. Synthesis of Highly Crystalline and Monodisperse Maghemite Nanocrystallites without a Size-Selection Process. *J. Am. Chem. Soc.* **2001**, *123*, 12798−12801.

(15) Hu, J.; Spotte-Smith, E. W.; Pan, B.; Herman, I. P. Improved Small-Angle X-Ray Scattering of Nanoparticle Self-Assembly Using a Cell with a Flat Liquid Surface. *J. Nanopart. Res.* **2019**, *21*, 71.

(16) X-Ray Attenuation Length. http://henke.lbl.gov/optical_constants/atten2.html (accessed on 8/26/2020).

(17) Narayanan, S.; Wang, J.; Lin, X.-M. Dynamical Self-Assembly of Nanocrystal Superlattices During Colloidal Droplet Evaporation by in Situ Small Angle X-Ray Scattering. *Phys. Rev. Lett.* **2004**, *93*, 135503.

(18) Smilgies, D.-M.; Heitsch, A. T.; Korgel, B. A. Stacking of Hexagonal Nanocrystal Layers During Langmuir−Blodgett Deposition. *J. Phys. Chem. B* **2012**, *116*, 6017−6026.

(19) Ershov, D.; Sprakel, J.; Appel, J.; Stuart, M. A. C.; van der Gucht, J. Capillarity-Induced Ordering of Spherical Colloids on an Interface with Anisotropic Curvature. *Proc. Natl. Acad. Sci. U. S. A.* **2013**, *110*, 9220−9224.

(20) Colosqui, C. E.; Morris, J. F.; Stone, H. A. Hydrodynamically Driven Colloidal Assembly in Dip Coating. *Phys. Rev. Lett.* **2013**, *110*, 188302.

(21) Berryman, J. G. Random Close Packing of Hard Spheres and Disks. *Phys. Rev. A: At., Mol., Opt. Phys.* **1983**, *27*, 1053.

(22) Wu, L.; Wang, X.; Wang, G.; Chen, G. In Situ X-Ray Scattering Observation of Two-Dimensional Interfacial Colloidal Crystallization. *Nat. Commun.* **2018**, *9*, 1−8.

(23) *CRC Handbook of Chemistry and Physics*, 101st ed.; Rumble, J. R., Ed.; CRC Press: Boca Raton, FL, 2020.

(24) Lemmon, E. W.; McLinden, M. O.; Friend, D. G. Thermophysical Properties of Fluid Systems. In *NIST Chemistry WebBook*; Linstrom, P. J., Mallard, W. G., Eds.; NIST Standard Reference Database Number 69; National Institute of Standards and Technology: Gaithersburg, MD, https://webbook.nist.gov (accessed on 8/26/2020).

(25) Peck, B.; Sigurdson, L. The Three-Dimensional Vortex Structure of an Impacting Water Drop. *Phys. Fluids* **1994**, *6*, 564−576.

(26) Gilet, T.; Mulleners, K.; Lecomte, J. P.; Vandewalle, N.; Dorbolo, S. Critical Parameters for the Partial Coalescence of a Droplet. *Phys. Rev. E* **2007**, *75*, 036303.

(27) Kaz, D. M.; McGorty, R.; Mani, M.; Brenner, M. P.; Manoharan, V. N. Physical Ageing of the Contact Line on Colloidal Particles at Liquid Interfaces. *Nat. Mater.* **2012**, *11*, 138−142.

(28) Colosqui, C. E.; Morris, J. F.; Koplik, J. Colloidal Adsorption at Fluid Interfaces: Regime Crossover from Fast Relaxation to Physical Aging. *Phys. Rev. Lett.* **2013**, *111*, 028302.

(29) Keal, L.; Colosqui, C. E.; Tromp, R. H.; Monteux, C. Colloidal Particle Adsorption at Water-Water Interfaces with Ultralow Interfacial Tension. *Phys. Rev. Lett.* **2018**, *120*, 208003.